

Supporting Information

Circumventing activity-selectivity trade-off via confinement effect from induced potential barriers on Pd nanoparticle surface

Junguo Ma^{a, †}, Chongya Yang^{b, †}, Xue Ye^{*c}, Xiaoli Pan^b, Siyang Nie^{*a}, Xing Cao^a, Huinan Li^a, Hiroaki Matsumoto^d, Liang Wu^e, and Chen Chen^{*a}

^a Engineering Research Center of Advanced Rare Earth Materials, Department of Chemistry, Tsinghua University, Beijing, P. R. China.

^b Dalian Institute of Chemical Physics, Chinese Academy of Science, Dalian, P. R. China.

^c College of Chemistry and Chemical Engineering, Yangzhou University, Yangzhou, P. R. China.

^d Hitachi High-Tech (Shanghai) Co., Ltd., Shanghai, P. R. China.

^e School of Chemistry and Chemical Engineering, Shanghai Jiao Tong University, Shanghai, P. R. China.

[†] These authors contributed equally: Junguo Ma, Chongya Yang.

Experimental Section/Methods

Catalyst preparation. The dorayaki-shaped ZnO particle were prepared with the hydrothermal method¹. Gelatin (3.0 g) and ultrapure water (600 mL) were sequentially added in a dry 1000 mL beaker. The mixture was stirred until the gelatin was fully dissolved, and then $\text{Zn}(\text{NO}_3)_2 \cdot 6\text{H}_2\text{O}$ (17.8 g) was added and dissolved, followed by hexamethylenetetramine (HMT) (8.4 g). The solution turned white and turbid, and was covered with a plastic wrap, and further stirred for 21 h at 80 °C. The white precipitate was washed with ultra-pure water and collected via centrifugation, and then dried, ground into powder, and calcined at 560 °C for 2 h to obtain ZnO powder, which served as a catalyst support.

The ZnO powder (1.0 g) was dispersed in ethanol (40 mL) under ultrasonication, forming a turbid suspension., add $\text{Pd}(\text{CH}_3\text{COO})_2$ (2.11 mg) was dissolved in acetone (10 ml), and the solution was added to the suspension. The mixture was further stirred at 60 °C in a water bath until all solvents were evaporated. The resulting solid was dried at 80 °C overnight and calcined for 3 h at 400 °C to obtain PdO/ZnO catalyst (mass fraction 0.1 wt%, determined via ICP-OES). The same method was used to prepare catalysts with other compositions.

Catalytic performance. The performance in C_2H_2 selective hydrogenation was assessed in a fixed-bed reactor at atmospheric pressure. The reactor was filled with PdO/ZnO catalyst (100 mg) with a mass fraction of 0.1 wt%, and quartz wool was used to fix the catalyst in both the upper and lower layers. Prior to the reaction, the catalyst was reduced in pure H_2 atmosphere at a certain temperature for 1 h, then cooled to room temperature and evaluated using a feed gas mixture of 2% C_2H_2 , 20% H_2 , and Ar balance at a gas flow rate of $18000 \text{ mL} \cdot \text{g}^{-1}_{\text{cat}} \cdot \text{h}^{-1}$. As this paper was focused on the hydrogenation mechanism of $\text{C}\equiv\text{C}$ into $\text{C}=\text{C}$, the selectivity for ethylene (C_2H_4) was examined. The conversion and selectivity were calculated according to the equations below:

$$X_{C_2H_2} = \frac{n_{C_2H_2(in)} - n_{C_2H_2(out)}}{n_{C_2H_2(in)}} \times 100\%$$

$$S_{C_2H_4} = \frac{n_{C_2H_4(out)}}{n_{C_2H_2(in)} - n_{C_2H_2(out)}} \times 100\%$$

where n_{in} and n_{out} represent the molar quantities of species at the inlet and outlet of the reactor, respectively.

Characterization. High-angle annular dark-field scanning transmission electron microscopy (HAADF-STEM) and high-resolution transmission electron microscopy (HRTEM) were conducted to characterize the metal particle size, morphology and microstructure of catalysts. A JEOL JEM-2100F electron microscope was used with 200 kV acceleration voltage. Ex situ TEM samples were prepared by dispersing a small amount of ground powder in anhydrous ethanol, sonicating and depositing 3–5 drops of the supernatant on a copper mesh grid. The grid was allowed to dry and then transferred to a vacuum sample chamber for testing.

In situ aberration-corrected scanning transmission electron microscopy (AC-STEM) on a Hitachi HF5000 electron microscope was employed to analyze selected regions of the sample with energy dispersive X-ray spectroscopy (EDS) and electron energy loss spectroscopy (EELS). The electron microscopy sample preparation involved dispersing the sample in ethanol, then depositing the obtained suspension onto a chip on the gas heating stage to enable observation via an electron transmission window. The in situ electron microscopy experiment involved loading the PdO/ZnO sample into the nano-reactor on the gas heating sample stage, connecting it to a flow gas device, introducing pure H₂ at room temperature, and heating to prescribed temperatures (e.g. 50 °C, 150 °C, and 300 °C) for 30 min. The TEM, EDS, and EELS data were collected before and after H₂ treatment at each temperature to observe the structural evolution of the PdO/ZnO catalyst.

The in-situ X-ray photoelectron spectroscopy (XPS) was conducted on a Thermofisher ESCALAB 250Xi spectrometer with monochromatic Al K α radiation ($h\nu = 1486.6$ eV, 15 kV, 10.8 mA). The sample, compressed into a pellet, was fixed on a conductive adhesive tape and pretreated with H₂ gas at temperatures of 50 °C, 150 °C, and 300 °C for 1 h before analysis. Surface charging effects were corrected using the C 1s peak (284.6 eV) from surface contaminating carbon as an internal standard. The data were analyzed and fitted with XPS PEAK software.

The H–D exchange experiment was performed on a Micromeritics AutoChem II 2920 chemisorption analyzer. The particle sample (100 mg, 20–40 mesh) was loaded into a U-shaped quartz tube and pretreated with high-purity hydrogen gas at temperatures of 50 °C, 150 °C, and 300 °C for 1 h. The system was then cooled to 30 °C before introducing H₂ and D₂ gases simultaneously. The temperature was ramped up to 300 °C at a heating rate of 5 °C min⁻¹ for the H–D exchange experiment. Thermal conductivity detector (TCD) was used to record the data, and mass spectrometry was used to analyze the components in the desorbed gas ($m/z = 2, 3, 4$).

The catalyst was characterized via in situ diffuse reflectance infrared Fourier transform spectroscopy (in situ DRIFTS) with a Bruker Equinox 55 Fourier transform infrared spectrometer. In situ DRIFTS at room temperature was conducted in absorbance mode with a resolution of 4 cm⁻¹, 64 scans, and a scanning range of 1000–4000 cm⁻¹. Powdered samples were loaded into an in situ cell, flattened, and reduced in H₂ atmosphere (20 mL min⁻¹) at 50 °C, 150 °C, or 300 °C for 1 h and then cooled to room temperature. Background spectra were collected and saved after purging with high-purity He for 0.5 h. The catalyst was then exposed to 20 vol% C₂H₂ or C₂H₄ (20 mL min⁻¹) until saturation, and the resulting infrared spectra were collected, representing the adsorption of C₂H₂ or C₂H₄ on the catalyst.

Computational details. All spin-polarized density functional theory (DFT) calculations were performed by using Vienna ab initio simulation package (VASP) with plane-wave pseudopotential.²⁻³ The cutoff of kinetic energy was 450 eV. The generalized gradient approximation (GGA) in the Perdew–Burke–Ernzerh of (PBE) functional were used to describe exchange and correlation energies.⁴ The projector-augmented wave (PAW) method was used to represent the core–valence interaction.⁵⁻⁷ The Brillouin zone was sampled with a $1 \times 1 \times 1$ k-points grid based on the Monkhorst–Pack scheme. The atomic positions were relaxed until the force on each atom was less than 0.01 eV/Å and electronic energies were converged within 10^{-4} eV. In order to describe the vdW interactions properly, a method with Becke–Johnson damping function was used.⁸

The initial structure was built according to the HRTEM results. Specifically, the optimized lattice constant (3.94 Å) of the bulky Pd₈ agrees well with the experimental value (3.89 Å).⁹ According to the lattice spacing value of 2.2454 Å corresponding to (111) plane, a Pd₂Zn₆ conventional cell was built by randomly substituting two Zn atoms in the optimized Pd conventional cell to simulate 150-Pd/ZnO sample. Similarly, a Pd₄Zn₄ conventional cell was also constructed to simulate 300-Pd/ZnO sample. For the calculations of thermodynamically parameters, the Special Quasirandom Structures (SQSs) of Pd₄Zn₄ with 2x2x2 super cell was found by GENSQS module within the Alloy Theoretic Automated Toolkit (ATAT).¹⁰⁻¹¹ The model has a vacuum of 15 Å along the Z-axis, which was large enough to avoid interaction between the slabs obtained after replication in the three space dimensions. Transition states were searched using the Climbing Image Nudged Elastic Band approach.¹² Frequency analysis was carried out to ensure that there was only a single imaginary frequency for the transition state.

Adsorption energies have been calculated according to the equation below:

$$E_{\text{ads}} = E_{\text{surf-X}} - (E_{\text{surf}} + E_{\text{X}})$$

where E_{surf} was the energy of slab, $E_{\text{surf-X}}$ was the total energy of the combined system (the adsorbate X bound to the substrate), E_{surf} was the energy of the substrate alone, and E_{X} was the total energy of the adsorbate in the gaseous phase.

Potential energy surface is important because it determines not only the diffusion barrier, but also the adsorption configuration. Here, we adopted the most stable surface of the PdZn alloy with the low-index (111). The potential energy surface was built by discrete points and using H atoms as detector (specifically, gridding the surface and calculating the adsorption energy of H atoms on the lattice). Then, the adsorption energies were drawn in the form of a contour map. It should be noted that, most of the adsorption sites were actually unstable, so we adopted the strategy of fixing the adsorbed molecules in x, y directions, and relaxing in the z direction to achieve the adsorption equilibrium.

Supporting Figures

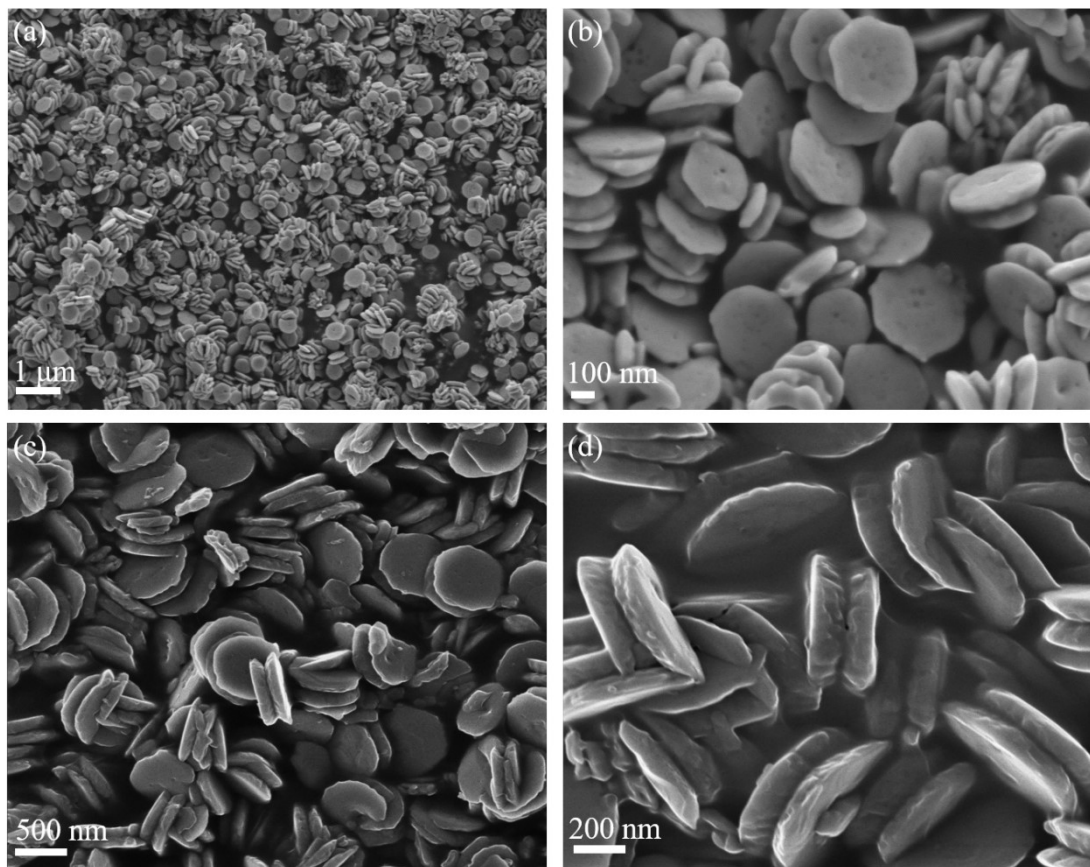


Figure S1. SEM images of ZnO support with a dorayaki-like morphology.

Note: The samples (c, d) were exposed in a HIM (Orion NanaFab, Carl Zeiss) to a 25 keV focused helium ion beam at a working distance of 8.52–8.55 mm. Helium pressure was maintained at 2×10^{-6} Torr during the exposure and a 5 μm beam limiting aperture was selected. A beam current of 1.46–1.47 pA was used to expose the large areas efficiently in the resist sensitivity evaluation.

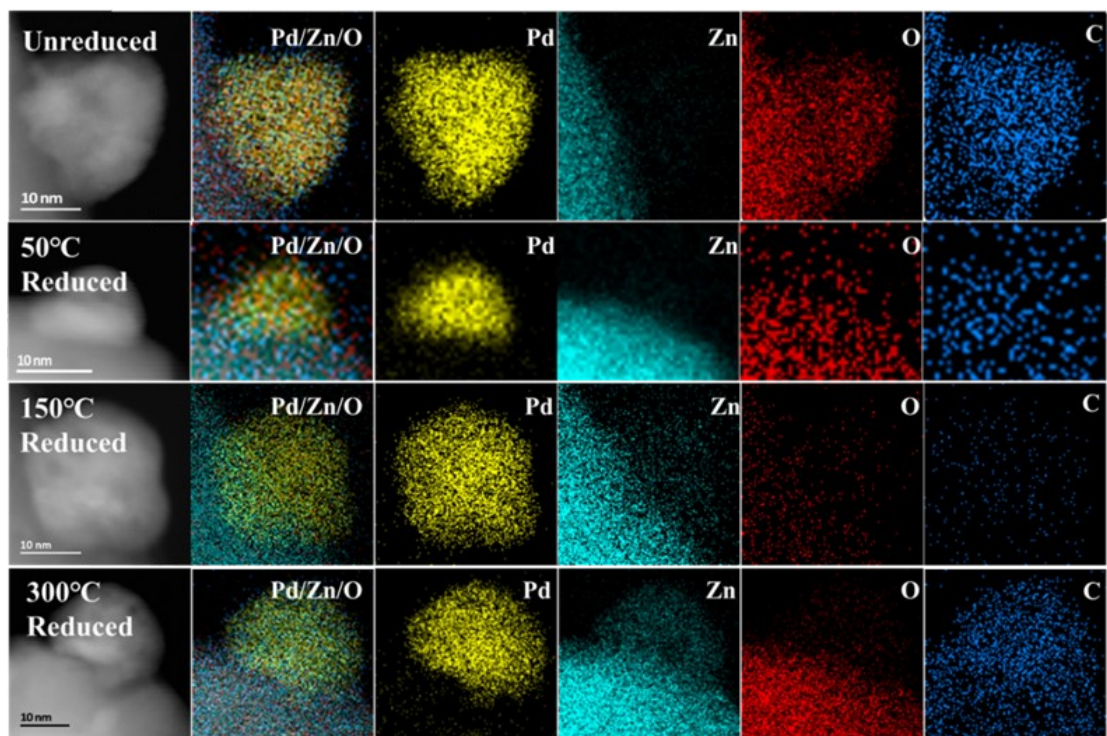


Figure S2. STEM images and corresponding elemental mapping of the Pd/ZnO catalyst series obtained under different reduction temperatures.

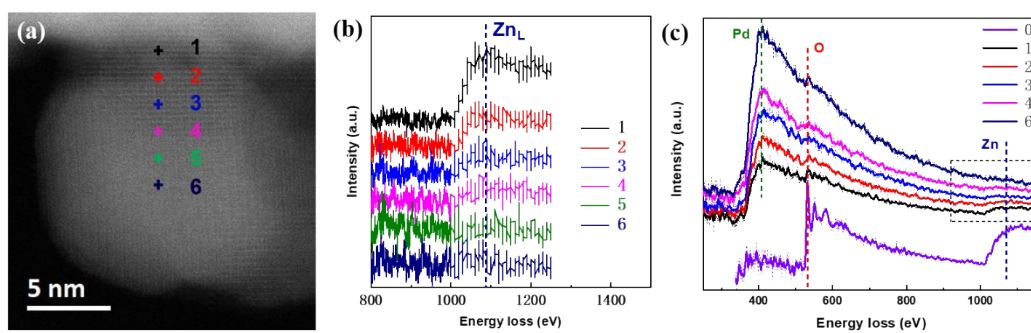


Figure S3. (a) In situ AC-STEM image of PdO/ZnO sample reduced under H₂ atmosphere. (b, c) The corresponding EELS profiles of Zn, O and Pd, in the numbered regions indicated in (a). Therein, dot O represents ZnO species.

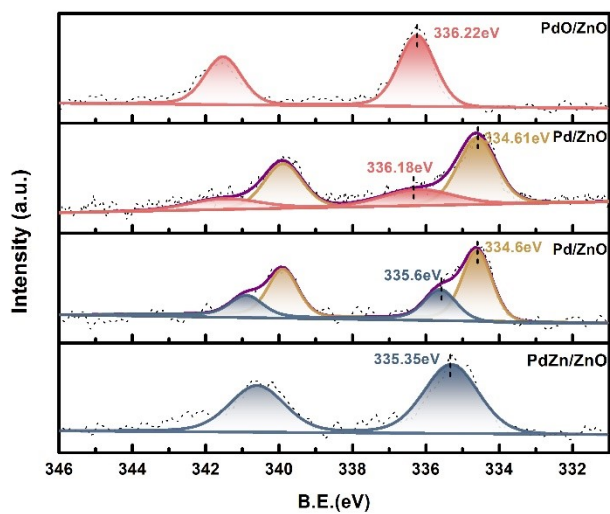


Figure S4. Fitted Pd 3d XPS profiles for PdO/ZnO, 50-Pd/ZnO, 150-Pd/ZnO, and 300-Pd/ZnO catalysts.

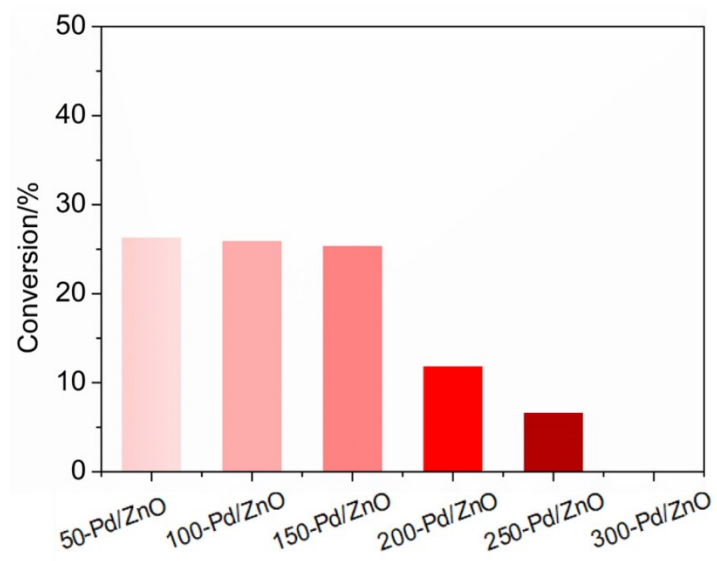


Figure S5. The intrinsic activity of series Pd/ZnO catalysts in C₂H₂ hydrogenation with varying reduction temperature. Reaction conditions: T < 20 °C, 0.05 g catalyst; 36,000 mL·g⁻¹_{cat}·h⁻¹.

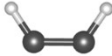
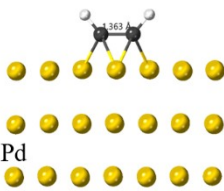
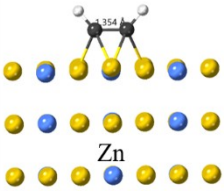
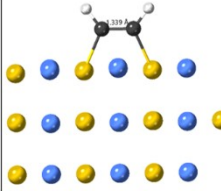
Sample	$C_2H_2(g)$	$C_2H_2-50-Pd/ZnO$	$C_2H_2-150-Pd/ZnO$	$C_2H_2-300-Pd/ZnO$
C-C	1.2 Å	1.363 Å	1.354 Å	1.339 Å
Model	~	$C_2H_2Pd_3$	$C_2H_2Pd_3$	$C_2H_2Pd_2$
Configuration				

Figure S6. Effect of Pd/ZnO catalysts on the C–C bond length and the adsorption configuration of C_2H_2 molecules.

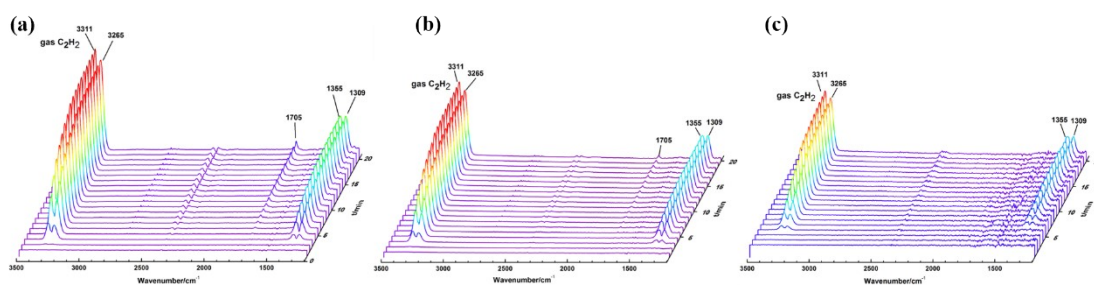


Figure S7. In situ C₂H₂-DRIFTS spectra presented for a series of Pd/ZnO catalysts reduced at (a) 50 °C, (b) 150 °C, and (c) 300 °C.

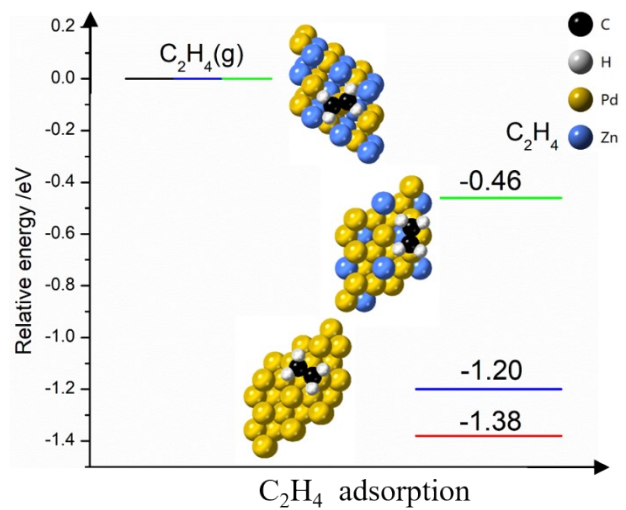


Figure S8. Energy diagrams for the C_2H_4 adsorption of 50-Pd/ZnO, 150-Pd/ZnO and 300-Pd/ZnO catalysts.

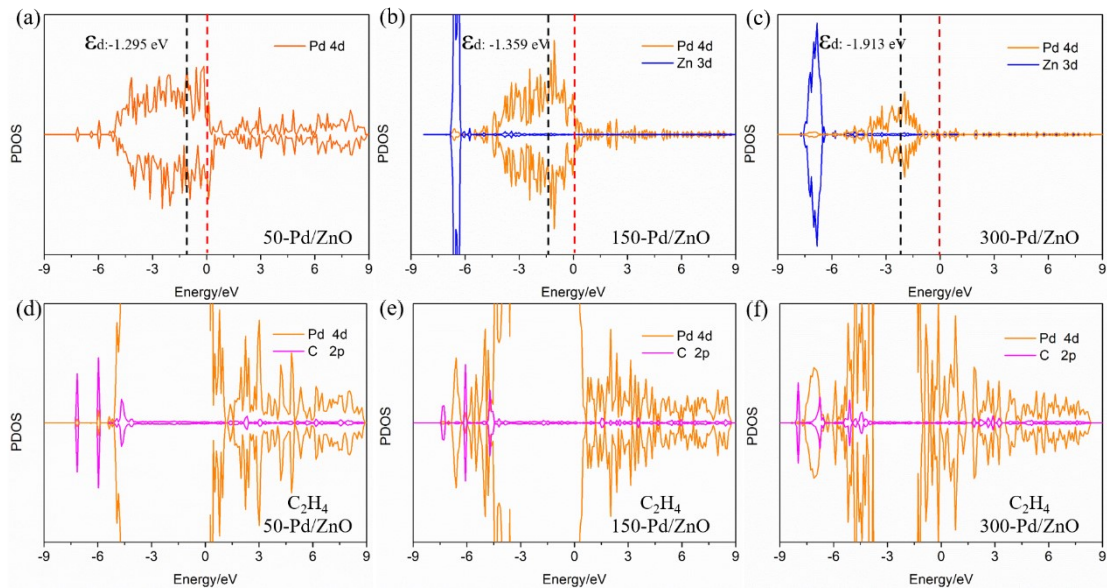


Figure S9. (a, b, c) PDOS of Pd 4*d* and Zn 3*d* for a series of Pd/ZnO catalysts reduced at different temperatures; (d, e, f) PDOS of Pd 4*d* and C 2*p* after C₂H₄ adsorption on the catalysts.

Note: Upon density of states (DOS) analysis, increasing Zn ratio in the catalyst leads to a shift of the d-band center of surface Pd atoms farther away from the Fermi level (Figure S9a–c), indicating a lower electron activity of Pd. Significant changes in the projected density of states (PDOSs) of the 4*d* orbitals of surface Pd atoms and the 2*p* orbitals of C₂H₄ C atoms are observed upon adsorption of C₂H₄ molecules on the three catalysts. Strong hybridization between the 4*d*_{xz} and 4*d*_{xy} orbitals of surface Pd atoms and the 2*p*_x and 2*p*_y orbitals of C₂H₄ C atoms is observed for 50-Pd/ZnO between –10.33, –7.17, –5.96 eV and –5.1 to –3.86 eV. However, for 300-Pd/ZnO (Figure S9d–f), a mismatch between the 4*d* orbitals of Pd atoms and the 2*p* orbitals of C₂H₄ C atoms in the density of states is rather prominent.

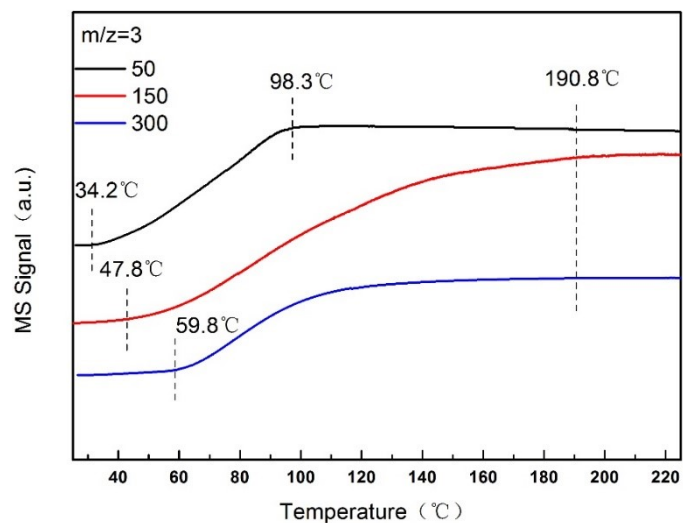


Figure S10. Results of the H–D exchange conducted on 50-Pd/ZnO, 150-Pd/ZnO, and 300-Pd/ZnO catalysts.

Supporting Tables

Table S1. Semi-quantitative analysis was performed on the EELS of Pd-*M* edge, O-*K* edge, and Zn-*L* edge corresponding to the numbered regions in Figure S4a.

Dot Element	0	1	2	3	4	6
Pd (M)	0	21%	52%	64%	78%	100%
O (K)	51%	41%	0	0	0	0
Zn (L)	48%	38%	48%	36%	22%	0
Pd:Zn	/	/	1.08:1	1.78:1	3.55:1	1:0

Table S2. The EELS of PdO/ZnO samples in unreduced state at room temperature and in situ reduced states at 300 °C and 500 °C.

Element	Reduction $T/^\circ\text{C}$		
	RT	300	500
Pd (M)	50%	84%	53%
O (K)	50%	0	0
Zn (L)	0	16%	47%
Pd:Zn	/	5.25:1	1.13:1

Table S3. Pd 3*d* XPS fitting results for catalysts containing PdO/ZnO, 50-Pd/ZnO, 150-Pd/ZnO, and 300-Pd/ZnO.

Sample	Pd ⁺		Pd ⁰		PdZn		Zn/Pd
	B.E. (eV)	Content	B.E. (eV)	Content	B.E. (eV)	Content	
PdO/ZnO	336.22	~100%					0
50-Pd/ZnO	336.20	32.7%	334.61	67.3%			0
150-Pd/ZnO			334.60	70.0%	335.60	30.0%	~ 1:5
300-Pd/ZnO					335.35	~100%	~ 1:1

Table S4. The C₂H₄ selectivity and C₂H₂ conversion rates of a series of Pd/ZnO catalysts reduced at different temperatures were recorded at reaction temperatures of 40 °C, 60 °C, 80 °C, and 100 °C. Pd/ZnO catalysts reduced at 300 °C were tested at reaction temperatures of 120–200 °C.

Reduction <i>T</i> /°C	Reaction <i>T</i> /°C								
	50	100	150	200	250	300			
	R _{C₂H₂}	S _{C₂H₄}		R _{C₂H₂}	S _{C₂H₄}	R _{C₂H₂}	S _{C₂H₄}	R _{C₂H₂}	S _{C₂H₄}
	(%)	(%)		(%)	(%)	(%)	(%)	(%)	(%)
40	34.17	64.32	90.16	38.27	96.61	17.25	92.70	~	~
60	16.26	45.18	73.05		94.28	52.95	97.66	4.86	86.19
80	16.74	38.35	68.50	100.00	92.23	99.32	98.08	13.78	91.34
100	21.56	42.28	69.41		91.22	100.00	96.34	42.62	97.55

Reduction <i>T</i> /°C	Reaction <i>T</i> /°C	
	300	
	R _{C₂H₂}	S _{C₂H₄}
	(%)	(%)
120	84.10	99.50
140	95.88	99.59
160	97.93	99.62
180	98.57	99.64
200	98.70	99.78

Table S5. Catalytic performances of different catalysts in semi-hydrogenation of acetylene.

Catalyst	Temp. (°C)	Space velocity (mL·gcat ⁻¹ ·h ⁻¹)	Feed (C ₂ H ₂ :H ₂)	Con.	Sel.	Note
Pd₂Ga	200	--	1:10	95	75	Armbrüster ¹³
AgPd_{0.01}/SiO₂	160	60000	1:10	67	87	Pei ¹⁴
PdZn/ZnO	60	180000	1:10	54%	88%	Zhou ¹⁵
PdZn/ZnO	150	180000	1:10	100%	91%	Zhou ¹⁵
PdIn/MgAl₂O₄	90	280000	1:10	96%	92%	Feng ¹⁶
PdZn@C/ZnO	140	--	--	95%	95%	Yang ¹⁷
Pd₁Cu₁/ND@G	110	--	--	~100%	92%	Huang ¹⁸
Au–Ni	RT	--	--	425 μmol·g ⁻¹ ·min ⁻¹	86%	Verma ¹⁹
DPC/RuPt-10-Calc	RT	--	--	320 mmol·g ⁻¹ ·h ⁻¹	90%	Sharma ²⁰
150-Pd/ZnO	40	180 00	1:10	~100%	90%	Table S4
200-Pd/ZnO	60	180 00	1:10	~100%	94%	Table S4
250-Pd/ZnO	80	180 00	1:10	99%	98%	Table S4
300-Pd/ZnO	160	180 00	1:10	98%	~100%	Table S4

CONTCAR

1.0000000000000000

11.1674003601000003 0.0000000000000000 0.0000000000000000

-5.7185515619000000 9.4963063314999996 0.0000000000000000

0.0000000000000000 0.0000000000000000 25.0000000000000000

Zn Pd

32 32

Selective dynamics

Direct

0.1577299982466727 0.4168100058936091 0.0040000002000014 F F F

0.8059628665020938 0.7341921329627271 0.1845701179349424 T T T

0.5536684883581853 0.4747660937657775 0.1854446349323405 T T T

0.8909100294103638 0.9060400127847359 0.0140300002000018 F F F

0.6180681571860277 0.6368179006940181 0.2764373236651455 T T T

0.2382699995972501 0.3352999985308003 0.0953200012399975 F F F

0.8831670009961755 0.6352150745021997 0.2811896661824672 T T T

0.9000499844297138 0.4135400056518250 0.0096599999999967 F F F

0.5525718247457974 0.7383034026693902 0.1859365071075353 T T T
0.3964399993262759 0.4045499861621664 0.0106300003999991 F F F
0.0514266739695424 0.7234146972794526 0.1892406926179220 T T T
0.7189000248885620 0.3243300020539124 0.0987700000399983 F F F
0.3688653294062528 0.6502852596438832 0.2709789887185867 T T T
0.9804599881063965 0.0769800022746878 0.0980599969600036 F F F
0.4010599851624832 0.9106400012934301 0.0086799999600018 F F F
0.0571794909466270 0.2364932438786079 0.1817844261491748 T T T
0.6585900187307914 0.9190499782057273 0.0073099998000004 F F F
0.3011592995684907 0.2303894224513374 0.1838445894103697 T T T
0.4751800000066453 0.8197399973480444 0.1011499986000004 F F F
0.1185230203135308 0.1302053872402779 0.2699179370960335 T T T
0.7307299971556702 0.8345699906195136 0.1001299992400035 F F F
0.3761238259255743 0.1433791917695510 0.2745190076522194 T T T
0.1359899938665023 0.9046900272690550 0.0082200001999979 F F F
0.7982766032868109 0.2345076689327704 0.1841556718444133 T T T
0.9736599922246683 0.8196200132236626 0.0981900021600026 F F F

0.6229889960049321 0.1361838609878211 0.2748586574345974 T T T
0.2193699926399972 0.8101800084606907 0.0992399975599980 F F F
0.8659506581128457 0.1237753011273162 0.2762183950072549 T T T
0.4813599884126489 0.0812700018364012 0.0995099991599986 F F F
0.1219617032659904 0.3913392896543470 0.2722506515247149 T T T
0.6506800055013855 0.6588100194543500 0.0102000003600011 F F F
0.2994041196358218 0.9766206206202601 0.1871450979867789 T T T
0.2281900048027552 0.5728899836512156 0.0975899994399967 F F F
0.8666290860258313 0.8693304808154972 0.2731492643243862 T T T
0.4973700046381282 0.5895799994812947 0.0972699969999979 F F F
0.1293413796463255 0.8929809905053734 0.2736648211613509 T T T
0.6455299854719669 0.1533199996055785 0.0080399997600011 F F F
0.3141709814219105 0.4747284974749610 0.1863452539903236 T T T
0.9036800265297131 0.1684200018584860 0.0118399998000029 F F F
0.9688199758459319 0.5707399845581733 0.0993100032399994 F F F
0.6190031241003451 0.8762281363817745 0.2746679459997672 T T T
0.1500300020176297 0.1594800055023882 0.0120200002399997 F F F

0.8062693152348530 0.4887312384225391 0.1913939691982927 T T T
0.3899799883746979 0.1382900029924130 0.0083200000400012 F F F
0.0485701963189711 0.4695902394024441 0.1872909879226429 T T T
0.6388400196568256 0.4090999960809327 0.0098700002000029 F F F
0.2968447375100721 0.7336794008918992 0.1847671325698806 T T T
0.4702999889413420 0.3204799890358316 0.0985699966400020 F F F
0.1239667129947256 0.6366144606829846 0.2761945268173489 T T T
0.1558299958445915 0.6720899939620892 0.0087200002800003 F F F
0.8111447450360266 0.9927196437032878 0.1855999413067180 T T T
0.4108299911078674 0.6780300140110356 0.0097300000400011 F F F
0.0526977361281907 0.9800175045076690 0.1825903365288110 T T T
0.7235699892020051 0.0763399973308907 0.0981900021600026 F F F
0.3585158157313638 0.3820043608139066 0.2835237044604808 T T T
0.2255800068227813 0.0517899989566075 0.0993599966000005 F F F
0.8668655303085669 0.3641033437609187 0.2760808092782952 T T T
0.8908200263544401 0.6554300188646991 0.0085899997599981 F F F
0.5513037700965920 0.9831145761861945 0.1851018259852902 T T T

0.5433913866644117 0.2281098779111984 0.1888551425412630 T T T

0.9792199730204914 0.3302699923017940 0.0959099978400033 F F F

0.7234699725786342 0.5656399726894179 0.1007499992799978 F F F

0.3796016484646532 0.9018691227431216 0.2749382630007655 T T T

0.6236998233970356 0.4003973373064846 0.27689898

References

1. Y.-H. Tseng, H.-Y. Lin, M.-H. Liu, Y.-F. Chen, C.-Y. Mou, *J Phys Chem C*. 2009, **113**, 18053–18061.
2. G. Kresse, J. Furthmüller, *Comp Mater Sci*. 1996, **6**, 15–50.
3. G. Kresse, J. Furthmüller, *Phys. Rev. B*. 1996, **54**, 11169.
4. J. P. Perdew, K. Burke, *Phys. Rev. Lett*. 1996, **77**, 3865.
5. P. E. Blochl, *Phys. Rev. B*. 1994, **50**, 17953–17979.
6. G. Kresse, D. Joubert, *Phys. Rev. B*. 1999, **59**, 1759.
7. O. Bengone, M. Alouani, P. Blochl, J. Hugel, *Phys. Rev. B*. 2000, **62**, 16392.
8. S. Grimme, *J. Comput. Chem*. 2006, **27**, 1787–1799.
9. J. Hu, W. Guo, Z. Liu, X. Lu, H. Zhu, F. Shi, J. Yan, R. Jiang, *J. Phys. Chem. C*. 2016, **120**, 20181–20191.
10. A. Zunger, S. H. Wei, L. G. Ferreira and J. E. Bernard, *Phys Rev Lett*, 1990, **65**, 353-356.
11. A. van de Walle, *Calphad*, 2009, **33**, 266-278.
12. G. Henkelman, B. P. Uberuaga, H. J. Jonsson, *Chem. Phys*. 2000, **113**, 9901.
13. M. Armbrüster, K. Kovnir, M. Behrens, D. Teschner, Y. Grin and R. Schlögl, *J Am Chem Soc*, 2010, **132**, 14745-14747.
14. G. X. Pei, X. Y. Liu, A. Q. Wang, A. F. Lee, M. A. Isaacs, L. Li, X. L. Pan, X. F. Yang, X. D. Wang, Z. J. Tai, K. Wilson and T. Zhang, *Acs Catal*, 2015, **5**, 3717-3725.
15. H. R. Zhou, X. F. Yang, L. Li, X. Y. Liu, Y. Q. Huang, X. L. Pan, A. Q. Wang, J. Li and T. Zhang, *Acs Catal*, 2016, **6**, 1054-1061.
16. Q. C. Feng, S. Zhao, Y. Wang, J. C. Dong, W. X. Chen, D. S. He, D. S. Wang, J. Yang, Y. M. Zhu, H. L. Zhu, L. Gu, Z. Li, Y. X. Liu, R. Yu, J. Li and Y. D. Li, *J Am Chem Soc*, 2017, **139**, 7294-7301.
17. L. N. Yang, Y. S. Guo, J. Long, L. X. Xia, D. Li, J. P. Xiao and H. Y. Liu, *Chem Commun*, 2019, **55**, 14693-14696.
18. F. Huang, M. Peng, Y. L. Chen, X. B. Cai, X. T. Qin, N. Wang, D. Q. Xiao, L. Jin, G. Q. Wang, X. D. Wen, H. Y. Liu and D. Ma, *J Am Chem Soc*, 2022, DOI: 10.1021/jacs.2c07208.
19. R. Verma, R. Tyagi, V. K. Vooora and V. Polshettiwar, *Acs Catal*, 2023, **13**, 7395-7406.
20. G. Sharma, R. Verma, S. Masuda, K. M. Badawy, N. Singh, T. Tsukuda and V. Polshettiwar, *Nat Commun*, 2024, 15.